RESEARCH PAPER

Fabrication and Ablation Behavior of a Novel 3D Orthogonal Woven C/C-SiC-HfC Composite by I-CVI, SI, and LSI Combined Process

Amin Rezaei Chekani[1], Malek Naderi[2,*], Reza Aliasgarian[3], Yousef Safaei[4]

* *mnaderi@aut.ac.ir*

[1] PhD Candidate, Department of Materials and Metallurgical Engineering, Amirkabir University of Technology, Tehran, Iran
[2] Full Professor, Department of Materials and Metallurgical Engineering, Amirkabir University of Technology, Tehran, Iran
[3] PhD, Department of Materials and Metallurgical Engineering, Amirkabir University of Technology, Tehran, Iran
[3] PhD Candidate, Isfahan University of Technology, Faculty of Material Engineering, Isfahan Province, IR 8415683111

Received: January 2026 **Revised: May 2026** **Accepted: June 2026**
DOI: 10.22068/ijmse.4552

Abstract: *A C/C-SiC-HfC composite was fabricated using a three-dimensional orthogonally woven (3DW) preform, and the effect of HfC ultra-high temperature ceramic (UHTC) particles on the microstructure and ablation properties of the composite was evaluated. First, pyrolytic carbon (PyC) was infiltrated into the 3DW preform by the isothermal chemical vapor infiltration (I-CVI) method. Then, impregnation of a suspension composed of HfC particles and phenolic resin into the 3DW preform. Next, liquid Si alloy was infiltrated into the C/C-HfC porous structure at 1650°C to form a C/C composite with a SiC-HfC matrix. HfC particles and the continuous SiC phase among carbon fibers were saturated, and during the oxyacetylene test, they covered the surface of the C/C-SiC-HfC composite as a dense, continuous SiO_2-HfO_2 layer. This layer acted as a barrier against the diffusion of oxygen into the bulk parts of the C/C-SiC-HfC composite. The results of the oxyacetylene flame test at 2500°C for 120 s showed that the mass and linear ablation rates of the C/C-SiC composite were 4.8 mg/s and 3.75 µm/s, respectively. After the addition of HfC and the formation of the C/C-SiC-HfC composite, these rates decreased to 1.6 mg/s and 0.98 µm/s, respectively.*

Keywords: *Three-dimensional orthogonally woven (3DW), Liquid silicon infiltration (LSI), C/C-SiC-HfC composite, Ablation behavior.*

1. INTRODUCTION

Increasing the speed of aerospace vehicles, especially hypersonic products, has resulted in the utilization of ultra-high temperature materials that exhibit appropriate oxidation and corrosion resistance at operating temperatures higher than 2000°C. In addition, propulsion applications require high shock resistance and mechanical strength at the above-mentioned temperatures since during the flight of hypersonic equipment in the atmosphere, a noticeable amount of heat is generated due to the friction present between these vehicles and the atmosphere, causing an increase in the surface temperature to temperatures higher than 2000°C [1-3]. At the beginning, researchers paid special attention to carbon-carbon composites as appropriate choices for applications in space and aerospace fields owing to their outstanding properties such as low density, low thermal expansion, proper mechanical properties at high temperatures, high specific strength and modulus, high thermal conductivity, and high shock and ablation resistance [4-7]. However, these materials are oxidized at temperatures >500°C, limiting their application at ultra-high temperatures [8]. Then, C/C-SiC composites received attention as proper candidates for thermal protection systems in the aerospace industry. C/C-SiC composites are also oxidized and degraded at temperatures >1700°C and are not viable for these conditions [9-11]. Therefore, C/C-SiC composites needed modifications to be proper choices in aerospace industries and be applied at ultra-high temperatures (>2000°C).

An effective method to modify C/C-SiC composites and utilize them at ultra-high temperatures is to use ultra-high temperature ceramics such as ZrC, ZrB_2, HfB_2 and HfC within the matrix of C/C-SiC composites. Among ultra-high temperature ceramics, HfC can be considered an effective material to enhance the ablation resistance of C/C-SiC composites because its melting point is 3827°C while that of HfO_2 is 2827°C. The presence of an oxide layer with such characteristics can act as a barrier against the diffusion of oxygen to the bulk layers of the composite, leading to a significant

[Downloaded from cehsat.iust.ac.ir on 2026-09-10]

[DOI: 10.22068/ijmse.4552]

increase in the ablation resistance of C/C-SiC composites [12-17]. However, the use of HfC is considered an ideal ultra-high temperature ceramic to be used in the matrix of C/C-SiC composites to fabricate C/C-SiC-HfC composites.

Preformed structures of C/C-SiC composites reinforced with ultra-high temperature ceramic particles include layered 2D and 3D preforms, which can be fabricated by methods such as braiding, weaving, stitching, knitting, and needle punching. Three-dimensional orthogonal preforms are one of the newest carbon preforms that were used in this study [18-20].

Various methods have been investigated to fabricate C/C-SiC composites reinforced with ultra-high temperature ceramic particles. Chemical vapor infiltration (CVI) [21, 22], polymer infiltration and pyrolysis (PIP) [23], slurry infiltration (SI) [20], and liquid silicon infiltration (LSI) [14] are among the most important and widely used methods to fabricate C/C-SiC composites reinforced with ultra-high temperature ceramic particles. The LSI process is a fast, cost-effective, and simple method that can be employed to fabricate high-density C/C-SiC-HfC composites reinforced with ultra-high temperature ceramic particles. Because of these reasons, it has been paid appreciable attention by researchers [24-27]. Duan et al. [14] fabricated a C/SiC-HfC composite by a combination of CVI, PIP, and LSI methods using $HfSi_2$ alloy powder and studied the ablation behavior of the composite through the oxyacetylene flame test for 20 s. With the fabrication of the C/SiC-HfC composite using the combined CVI, PIP, and LSI methods, the mass and linear ablation rates of the C/SiC composite decreased from 12 mg/s and 8.3 μm/s to 2.9 mg/s and 2.2 μm/s, respectively. Liu et al. [28] evaluated the fabrication and ablation resistance of the C/C-HfC-SiC in-situ composite through a combination of CVI and LSI methods using a mixture of Al_2O_3 and $HfSi_2$ powders. The mass and linear ablation rates of this composite decreased significantly compared with those of the C/C-SiC composite.

Generally, most of the studies performed on C/C composites have used 2D preforms, traditional fabrication methods, and reactive starting materials, leading to the fabrication of C/C-SiC-HfC in-situ composites [29-31]. To the best of our knowledge, there has been no research on the investigation of the ablation resistance of C/C-SiC-HfC composites fabricated by HfC particles using 3D orthogonal preforms through the I-CVI, SI, and LSI combined method.

In this research, a C/C-SiC-HfC composite using a three-dimensional orthogonally woven preform, ultra-high temperature HfC ceramic particles, and I-CVI, SI, and LSI combined method has been fabricated, and its ablation behavior has been assessed. The I-CVI, SI, and LSI combined method is a fast, cost-effective, and novel technique to fabricate C/C-SiC-HfC composites. First, a large amount of HfC particles was loaded into a porous C/C preform by the SI method, followed by the infiltration of liquid Si alloy into a porous structure of C/C-HfC at 1650°C to form a C/C-SiC-HfC composite. The SiC phase forms in a continuous and relatively uniform way in the matrix structure by the reaction between carbon sources and liquid Si alloy during the LSI process. Ultimately, the microstructure and ablation behavior of the C/C-SiC-HfC composite are investigated. The selection of HfC powder (1–5 μm) over reactive Hf-containing alloys was primarily driven by the following considerations:

- **Enhanced microstructural homogeneity:** Utilizing HfC powder allows for a more uniform distribution of the HfC phase within the matrix compared to reactive Hf-containing alloys. In reactive synthesis, the localized reaction kinetics often lead to heterogeneous distribution or clustering of the reinforcing phase. By employing pre-synthesized HfC powder, we achieved a more controlled and homogeneous dispersion.
- **Higher phase fraction control:** The use of HfC powder enables a precise and higher weight fraction of the HfC phase within the matrix. In contrast, reactive approaches are often constrained by stoichiometric limitations or the incomplete conversion of reactants, making it difficult to attain a high, stable volume fraction of the reinforcement phase.

2. EXPERIMENTAL PEOCEDURES

Fig. 1 shows the fabrication flow chart for the preparation of the C/C-SiC-HfC composites via the combined process of I-CVI, SI, and LSI. A 3DW preform made of T-300 (6K) carbon fibers, with a density of 0.67 g/cm³, dimensions of 67 × 43.50 × 47.40 mm, and a fiber volume fraction of 40%, was used in this work. Carbon matrix was introduced into the 3DW preform by

[Downloaded from cehsat.iust.ac.ir on 2026-09-10]

[DOI: 10.22068/ijmse.4552]

I-CVI at 1050°C using methane (CH_4) as precursor to form a porous C/C skeleton, followed by a graphitization process at 2400°C for 1 hr. The density of the 3DW preform was reached 1.06 g/cm^3 with an open porosity of 42%. HfC powder (1-5 µm, 99.99% purity, China), phenolic resin (THC-800, purity: 95.0%, China), and ethanol solution were used to prepare a high-solid-loading HfC by planetary ball milling with ZrO_2 balls for 6 hrs. Fig. 2 depicts the morphology and XRD pattern of the particles of HfC. Subsequently, the slurry was impregnated into the 3DW carbon fabric in a desiccator with a vacuum pressure of -0.7 bar for 45 min. Afterwards, the preform was placed into an autoclave under a constant pressure of 20 bar and temperature of 170°C for 2 hrs. In the SI process, the optimal sample exhibited a relatively uniform distribution of HfC particles within the matrix structure, corresponding to approximately 20 wt.% HfC. Phenolic resin was used to supply a carbon source and fix the HfC, followed by pyrolysis and thermal treatment under a continuous argon flow at 1050°C and 2400°C for 2 hrs respectively. As a result, a C/C-HfC composite with a density of 1.18 g/cm^3 was obtained by repeating the impregnation-pyrolysis process 3 times. The 3DW preform was placed in a graphite crucible with Si powder and heated to 1650°C for 3hrs in a vacuum atmosphere under a constant pressure of 10^{-2} bar for the LSI process to take place. At temperatures above the melting point of silicon (T_m= 1415°C), the fluidity of the liquid silicon increases, facilitating its infiltration into microcracks formed during the carbonization process. The molten Si was infiltrated into the preform by capillary forces along the carbon fibers, where it reacted with the carbon source to form the SiC matrix. Concerning the T300 (K6) carbon fibers employed in the present study, as well as the preform fabrication method used to generate a dense and structurally robust three-dimensional orthogonal architecture, the fibers exhibited negligible degradation during molten Si infiltration. The compact preform configuration is expected to restrict excessive penetration of molten silicon and thereby mitigate direct fiber attack. This observation is supported by the SEM results, which revealed that the carbon fibers largely preserved their morphology and structural integrity, with no evident signs of severe degradation. The phase composition of the C/C-SiC-HfC composite was identified using an X-ray diffractometer (XRD; GNR, Italia) with CuKα1 radiation at room temperature. The density and open porosity of the specimens were averaged over 5 measurements by Archimedes' method.

The ablation test was performed by averaging three measurements. The specimen features were assessed using an oxyacetylene torch. The pressure and flux of C_2H_2 were 0.095 MPa and 0.31 L/s, and for O_2 were 0.4 MPa and 0.42 L/s, respectively. The specimens were exposed to the flame for 120 s. The internal diameter of the tip of the nozzle was 2.0 mm, and the distance between the samples and the nozzle tip was 10 mm. As detected by an optical pyrometer, the surface temperature of the sample center reached 2500°C.

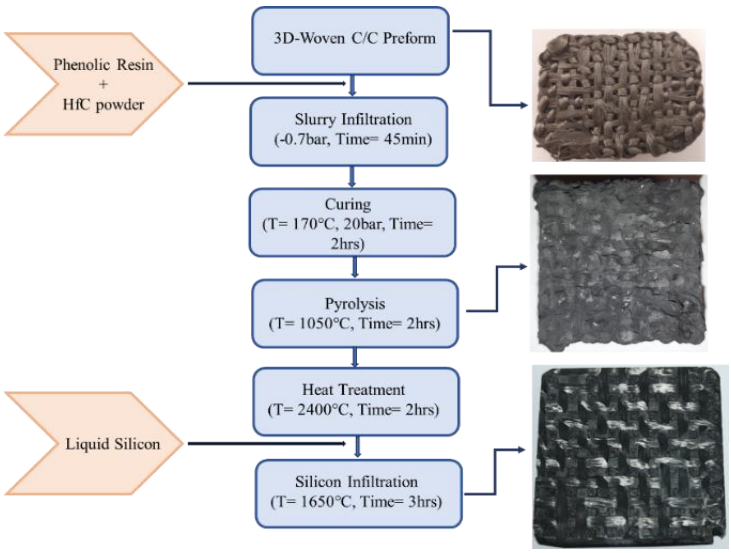

Fig. 1. Flow chart for the process of fabricating C/C-SiC-HfC composites by the combined process of I-CVI, SI and LSI

[Downloaded from cehsat.iust.ac.ir on 2026-09-10]

[DOI: 10.22068/ijmse.4552]

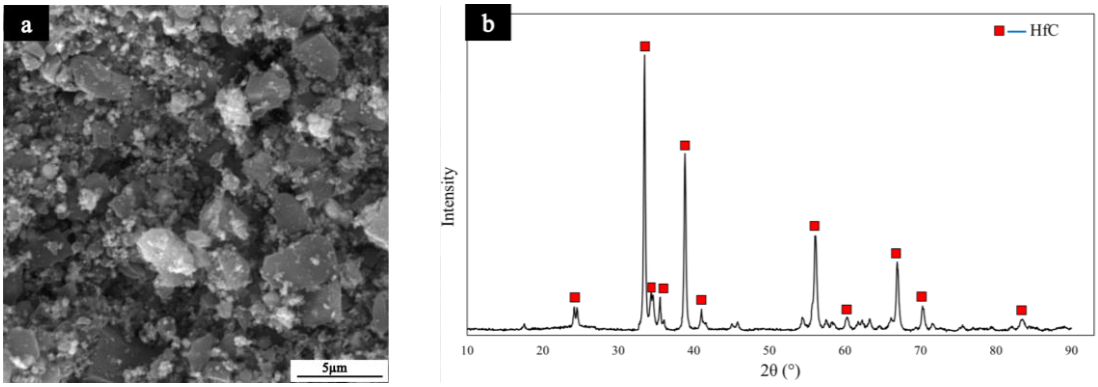

Fig. 2. The morphology and X-ray diffraction pattern of HfC powder.

The linear and mass ablation rates of the tested samples were calculated using Eqs. (1) and (2), respectively:

$R_l = (d_0 - d_1)/t$ (1)

$R_m = (m_0 - m_1)/t$ (2)

where R_l is the linear ablation rate; d_0 and d_1 are the thickness values of samples in the center region before and after ablation, respectively; R_m is the mass ablation rate; m_0 and m_1 are the masses of the samples before and after ablation, respectively; t is the ablation time. The microstructure and elemental distribution of the composites were examined using a field emission scanning electron microscope (FESEM) and an energy dispersive spectroscope (MIRA3, TESCAN, Czech).

3. RESULTS AND DISCUSSION

3.1. Microstructure of As-Fabricated C/C–SiC-HfC Composite

Table 1 shows the density and porosity percentage of the as-fabricated composites in this study, including C/C-SiC and C/C-SiC-HfC by the I-CVI, SI, and LSI combined method, compared with C/C-SiC-HfC composites [14] and C/C-SiC-HfC composites [28] through the combined LSI, PIP, CVI and LSI, CVI method. When the density and porosity percentage of C/C-SiC (1.92 g/cm^3), C/C-SiC-HfC (2.61 g/cm^3) [14], C/C-SiC-HfC [28] (2.32 g/cm^3), and C/C-SiC-HfC (2.68 g/cm^3) composites are compared, it can be found that the C/C-SiC-HfC composite (2.68 g/cm^3) exhibits the highest density and the lowest porosity percentage. The reason can be related to the direct impregnation of a high solid loading of HfC by the SI process into the C/C porous structure, the infiltration of liquid Si alloy, and its reaction with both carbon sources and carbon fibers of the preform, and consequently, the formation of a continuous ceramic SiC phase in the structure of the composite matrix during the novel I-CVI, SI, and LSI combined method. In general, the impregnation of a high amount of high-density HfC solid particles by the SI process in addition to the infiltration of liquid Si alloy at 1650°C within the porous matrix of the composite, leads to the filling of the preform and obtaining a high-density C/C-SiC-HfC composite with a low porosity percentage. The LSI method is cost-effective, fast, and efficient, producing C/C-SiC composites with high densities and low porosity percentages reinforced with ceramic particles. Nowadays, this method has attracted considerable attention [14, 28].

Fig. 3(a, b) shows the microstructure of the C/C-SiC-HfC composite fabricated by the novel C-C preform and the new I-CVI, SI, and LSI combined method. As can be seen in Fig. 4, ultra-high temperature HfC ceramic particles (white points) have uniform distributions in the composite structure. This is because of using a new fabrication method as well as a novel preform, which in turn, causes both higher penetration and stabilization of HfC particles in the matrix structure. These particles are trapped by phenolic resin among carbon fibers during the impregnation process and are stabilized during the curing process.

Table 1. Density and porosity percentage of C/C-SiC, C/C-SiC-HfC [28], C/C-SiC-HfC [14], and C/C-SiC-HfC composites

Composites	C/C-SiC	C/C-SiC-HfC [28]	C/C-SiC-HfC [14]	C/C-SiC-HfC
Density (gr/cm^3)	1.92	2.32	2.61	2.68
Porosity (%)	20.5	13.4	17.4	12

[Downloaded from cehsat.iust.ac.ir on 2026-09-10]

[DOI: 10.22068/ijmse.4552]

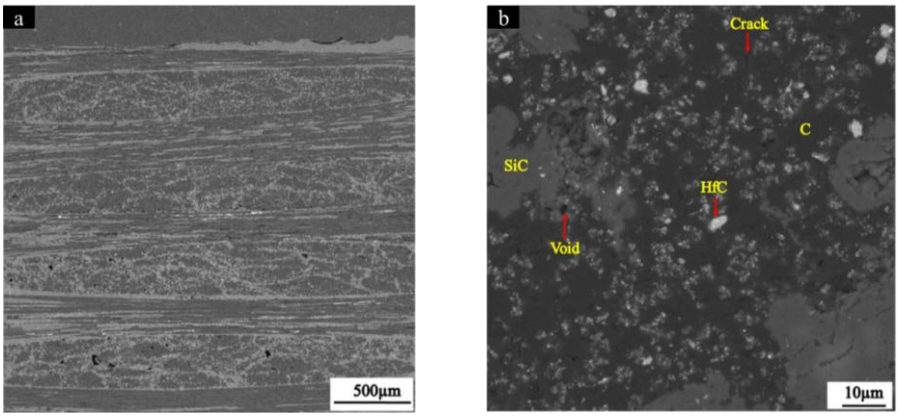

Fig. 3. Micrograph of the cross-section of the C/C-SiC-HfC composite

Furthermore, the SiC ceramic phase is distributed within the matrix in a continuous layered form through the reaction of carbon sources and carbon fibers with liquid Si alloy, creating a relatively uniform structure. The presence of microcracks in the C/C-SiC-HfC composite fabricated by the new I-CVI, SI, and LSI combined method can be explained by the reaction between the carbon fibers of the 3DW preform and the liquid Si alloy at a high temperature (1650°C), which is an extremely exothermic reaction. In addition, the difference in the thermal expansion coefficients of HfC, SiC, and C/C composite, which are $6.6 \times 10^{-6}\,K^{-1}$, $4 \times 10^{-6}\,K^{-1}$, and $2 \times 10^{-6}\,K^{-1}$, respectively, is another important factor that affects the formation of microcracks in the structure of the C/C-SiC-HfC composite [14, 28].

The details of the microstructure of the C/C-SiC-HfC composite can be found in Fig. 4(a, b). As can be seen, the space between carbon fibers of the 3DW preform is filled with four different colors: dark gray, light gray, mild gray, and white, which show C, Si, SiC, and HfC, respectively. The as-fabricated composite exhibits a dense matrix (with a high density) containing SiC and HfC ceramic phases with a limited number of microcracks and macroporosities. Fig. 4(a, b) obviously shows that the distribution of HfC particles within the matrix of the C/C-SiC-HfC composite is noticeably uniform. The results of the EDS analysis of various points of the C/C-SiC-HfC composite can be seen in Fig. 4(c, d, e, and f). Point 1 depicts the HfC particles located in the center of the C/C-SiC-HfC composite (Fig. 4c), which confirms the uniform distribution of HfC particles in Fig. 4a. Point 2, which is near the carbon sources (caused by the pyrolysis of phenolic resin) and carbon fibers, consists of the SiC continuous ceramic phase, which is the result of an exothermic reaction between carbon and the liquid Si alloy at 1650°C (Fig. 4d). It is clear in Fig. 4b that the regions with a light gray color (Si) are located in the center of the regions with a mild gray color (SiC). This shows that the reaction between carbon and liquid Si alloy at 1650°C has been incomplete, with an increase in the distance from the regions that are rich in carbon. Point 4 shows the carbon sources that were generated because of the pyrolysis of phenolic resin, which play a crucial role in the formation of the SiC continuous phase (Fig. 4f).

Fig. 5 shows the SEM-BSE microstructures of the C/C-SiC-HfC composite of the light gray and mild gray regions, in detail. As mentioned above, with an increase in the distance from the regions rich in carbon, the chemical reaction between carbon and liquid Si alloy at 1650°C decreases or occurs in an incomplete form (Fig. 5 c, d). Thus, since the results of this research show that the residual Si in the C/C-SiC-HfC composite results in degraded ablation resistance, it is recommended that the preform should be designed such that a minimum distance between carbon sources and liquid Si alloy is achieved (with a minimum size of pores). The XRD pattern of the as-fabricated C/C-SiC-HfC composite is shown in Fig. 6. The main crystalline phases detected in the C/C-SiC-HfC composite are HfC, SiC, and C (the composite consists of 76 wt.% carbon, 20 wt.% HfC, and 4 wt.% Si.). Moreover, a minor amount of Si can also be seen, which agrees with the incomplete reaction between carbon and silicon. Although LSI is cost-effective, fast, and efficient, there is always a minor amount of Si in the structure of carbon-carbon composites reinforced with ultra-high temperature ceramic particles, leading to decreased ablation resistance of the composite.

[Downloaded from cehsat.iust.ac.ir on 2026-09-10]

[DOI: 10.22068/ijmse.4552]

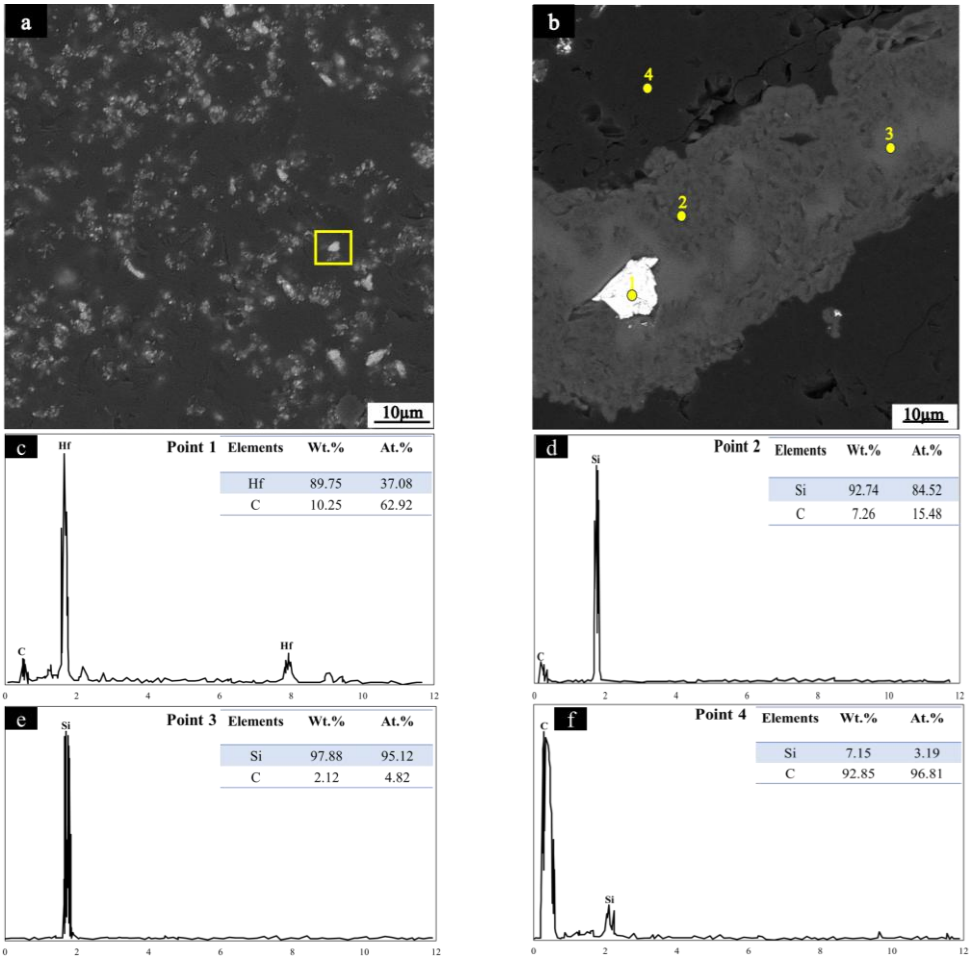

Fig. 4. a,b) SEM-BSE micrographs of the cross-section and c-f) EDS analysis of various points of the C/C-SiC-HfC composite

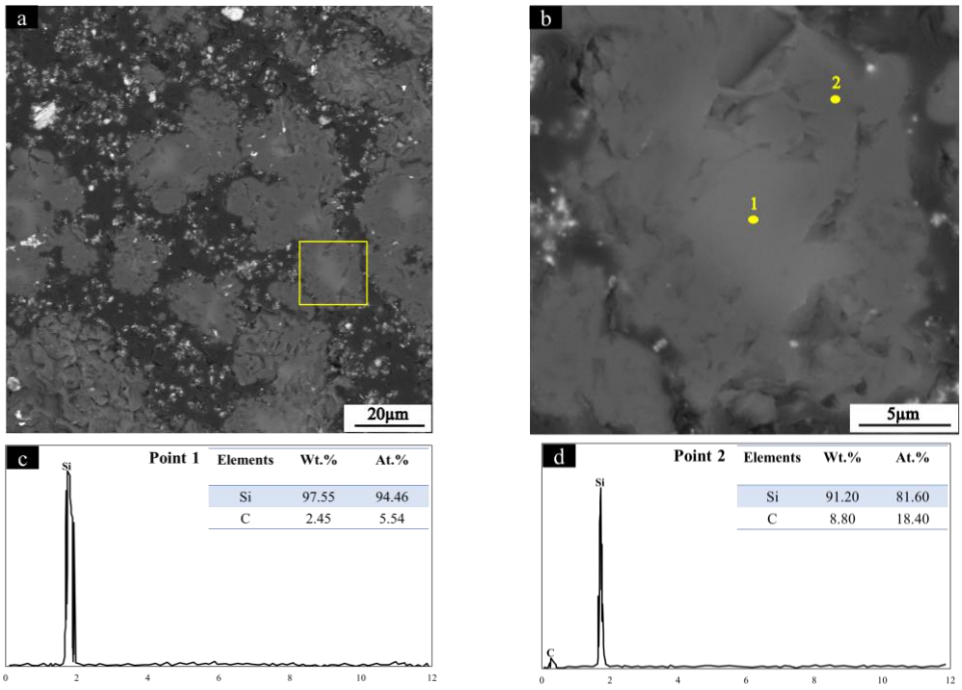

Fig. 5. a,b) SEM-BSE micrographs and c,d) EDS analysis of various points of the C/C-SiC-HfC composite

[Downloaded from cehsat.iust.ac.ir on 2026-09-10]

[DOI: 10.22068/ijmse.4552]

The presence of HfC, SiC, and C phases in the XRD pattern of the C/C-SiC-HfC composite is in agreement with the results of the EDS analysis (Fig. 4c-f).

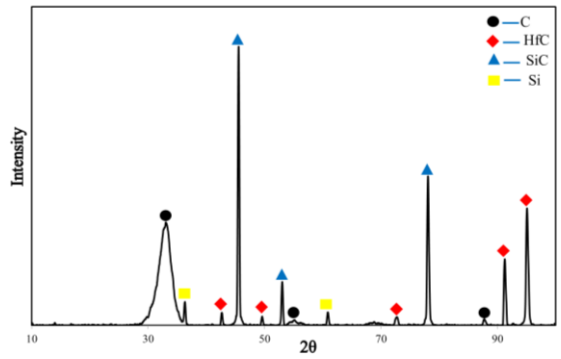

Fig. 6. XRD pattern of the C/C-SiC-HfC composite

3.2. Formation Mechanism of the C/C–SiC–HfC Composite

Fig. 7 demonstrates the schematic evolution mechanism of the C/C-SiC-HfC composite fabricated through the I-CVI, SI, and LSI combined method using the novel 3DW preform. At first, the pyrolytic carbon layer forms on the carbon fibers through the I-CVI process. Then, liquid Si alloy is infiltrated into the porous 3DW carbon-carbon preform containing ultra-high temperature HfC particles, leading to the formation of the SiC crucial continuous phase by solving carbon atoms and reacting with liquid Si alloy. Next, HfC particles, which are not stabilized by phenolic resin, rearrange by the surface tension of liquid Si alloy, resulting in the formation of large, continuous HfC clusters. It has been shown that the presence of liquid Si alloy among ultra-high ceramic temperature particles with different sizes can increase mass transfer along with the ease of migration to grain boundaries [14]. Over time, finer HfC particles are dissolved within HfC clusters, penetrate the melt, and crystallize in coarser particles, creating an irregular space among growing HfC particles. In brief, although HfC particles do not affect the reaction between carbon and liquid Si alloy, the uniform distribution of HfC particles within the C/C-SiC-HfC composite is not influenced by liquid Si alloy.

3.3. Ablation Resistance Behavior of C/C-SiC-HfC Composite

Fig. 8 shows the macrostructures of the C/C-SiC-HfC composite before and after the ablation test at 2500°C for 120 s. The sample that was under the oxyacetylene flame test for 120 s, had dimensions of 25 mm× 25 mm × 25 mm (Fig. 8a). Ablation tests were performed on three distinct samples, with the reported values representing the mean of the three individual ablation measurements. After the ablation test, the surface coating formed on the sample surface is divided into three distinct regions: edge region (C), transitional or middle region (B), and central region (A) (Fig. 8b). A white region can be seen on the surface of the C/C-SiC-HfC composite under the oxyacetylene flame test. The area and thickness of this white layer increase with an increase in the test time to 120 s. This layer is composed of oxide products of the first constituents of the C/C-SiC-HfC composite.

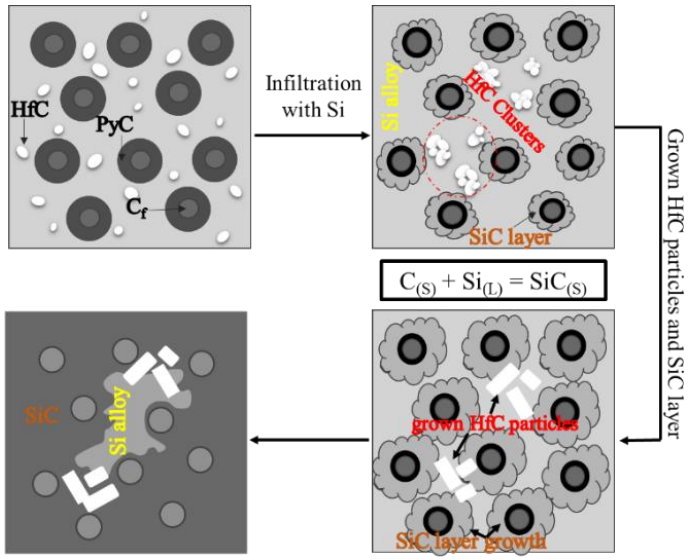

Fig. 7. Microstructure and process of the formation of the C/C-SiC-HfC composite during LSI

[Downloaded from cehsat.iust.ac.ir on 2026-09-10]

[DOI: 10.22068/ijmse.4552]

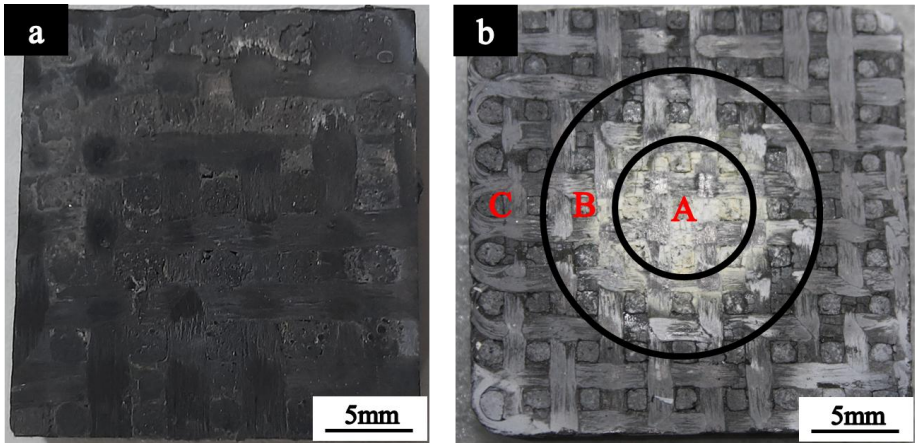

Fig. 8. Macrographs of the C/C-SiC-HfC composite a) before and b) after the oxyacetylene flame test

The highest ablation rate occurs in the central region of the sample since the pressure and temperature of the oxyacetylene gas are at their maximum values. When the C/C-SiC-HfC composite is subjected to the oxyacetylene gas at 2500°C for 120 s, SiO_2 and HfO_2 phases form on the sample surface with a white color.

To determine the mass and linear ablation rate, first, the dimensions (thickness) and weight of the samples were accurately measured before and after the oxyacetylene flame test using a digital micrometer and a 0.0001 gr balance. Table 2 shows the charts of the mass and linear ablation rates of the as-fabricated samples in this study (C/C-SiC and C/C-SiC-HfC), compared with those reported in the almost similar research conducted by Duan et al. [14]. As can be seen, the mass and ablation rates of the C/C-SiC-HfC composite are significantly higher than those of the C/C-SiC and C/C-SiC-HfC [14] samples. The weight of the samples after the oxyacetylene flame test decreases owing to the formation and evaporation of oxide products at the high temperature of the flame (about 2500°C) and the long test duration (120 s). Under these conditions, some oxide products such as CO, CO_2, SiO, and SiO_2 evaporate and are released from the sample surface. Among the samples, the C/C-SiC-HfC composite exhibits the highest ablation resistance under the oxyacetylene flame conditions. This can be related to the addition of a high amount of HfC ultra-high temperature ceramic particles and their relatively uniform distribution within the porous 3DW C/C through the SI process. HfC particles transform into a dense oxide layer of HfO_2 at the high flame temperature (around 2500°C) and the long exposure time (120 s). This white surface layer acts as a strong barrier against the diffusion of oxygen to the bulk layers of the C/C-SiC-HfC composite, leading to a decrease in the mass and linear ablation rates and, in general, increasing the oxidation and ablation resistance of the C/C-SiC-HfC composite.

Fig. 9(a-f) shows the SEM-BSE microstructures and EDS analysis of the microstructure of the central, transition, and side regions of the C/C-SiC-HfC composite exposed to the oxyacetylene flame for 120 s. In the central region of the sample, where maximum temperature and pressure exist, SiC and HfC carbide phases are rapidly oxidized and convert into SiO_2 and HfO_2, respectively. With increasing the oxyacetylene flame time, SiO_2 gradually evaporates, leading to the formation of microporosities on the surface of the C/C-SiC-HfC composite along with an increase in the mass ablation rate. The presence of surface micro-porosities, which are obviously seen in Fig. 9a, is due to the evaporation of SiC and C. The analysis result of the central region (Fig. 9b) confirms that the white surface layer is HfO_2. Fig. 9c depicts the surface morphology of the transitional or middle region. It can be seen that the composite surface in the transitional region consists of a coating of white and gray rough porous glass phases.

Table 2. Mass and linear ablation rates of the C/C-SiC-HfC, C/C-SiC-HfC [14] and C/C-SiC composites

Composites	C/C-SiC	C/C-SiC-HfC [14]	C/C-SiC-HfC
Mass ablation rate (mg/s)	4.8	2.6	1.6
Linear ablation rate (µm/s)	3.75	-	0.98

[Downloaded from cehsat.iust.ac.ir on 2026-09-10]

[DOI: 10.22068/ijmse.4552]

The EDS analysis of the middle region (Fig. 9d) shows the presence of a layer consisting of combined SiO_2 and HfO_2 phases. This combined glass layer inhibits the oxidation and ablation of the C/C-SiC-HfC composite. Since the temperature of the middle region is lower than that of the central region, the amount of Hf is lower than that of Si, as shown in the EDS analysis. The presence of surface microporosities, seen in Fig. 9b, is because of the evaporation of SiC and C. In the edge region, the sample surface is gray (Fig. 9f). The EDS analysis of this region shows the presence of a Si-Hf-O ternary compound with Si and O as the major constituents, demonstrating the formation of the SiO_2 phase. In this region, the amount of the HfO_2 phase is very small because of the relatively lower temperature of this region compared with that of the central and middle regions. Fig. 10 depicts the SEM-BSE microstructure and the EDS map of the C/C-SiC-HfC composite from the edge region (C) toward the central region (A). According to the SEM-BSE microstructure, the volume fractions of Hf and O elements increase gradually from region C toward region A, while the volume fraction of Si and O elements increases gradually from region A toward region C. This is due to the temperature gradient of regions A and C. Region C has the minimum pressure, velocity, and temperature of the oxy-acetylene flame, whereas these parameters are all maximum in region A, and thus, the formation of the HfO_2 glass phase increases from region C toward region A. Also, comparing the EDS analysis of Fig. 9(b, f) with the XRD pattern in Fig. 13 confirms the formation of HfO_2 mainly in region A. The dense HfO_2 oxide layer acts as a strong barrier against the diffusion of oxygen to the bulk layers of the C/C-SiC-HfC composite, leading to an increase in both the oxidation and ablation resistance of the composite to a great extent.

Fig. 11 displays the XRD pattern of the central region (A) of the C/C-SiC-HfC composite after the oxyacetylene flame test. This pattern belongs to the SEM microstructure (Fig. 9a) of the C/C-SiC-HfC composite with a white layer. The XRD pattern of Fig. 11 shows that the melted white layer in this region is HfO_2 oxide phase, caused by the oxidation of HfC particles during the ablation test. HfO_2 remains stable until the end of the oxyacetylene flame test owing to its higher melting point (2785°C). However, SiO_2 rapidly evaporates at 2500°C and exits the surface because of the high pressure of the oxyacetylene gas in the central region (the presence of micro-porosities in the central region in Fig. 8a) [29].

3.4. Ablation Mechanism

Ablation testing under an oxyacetylene gas flame is a very complicated process, which probably consists of kinetic and thermodynamic phenomena.

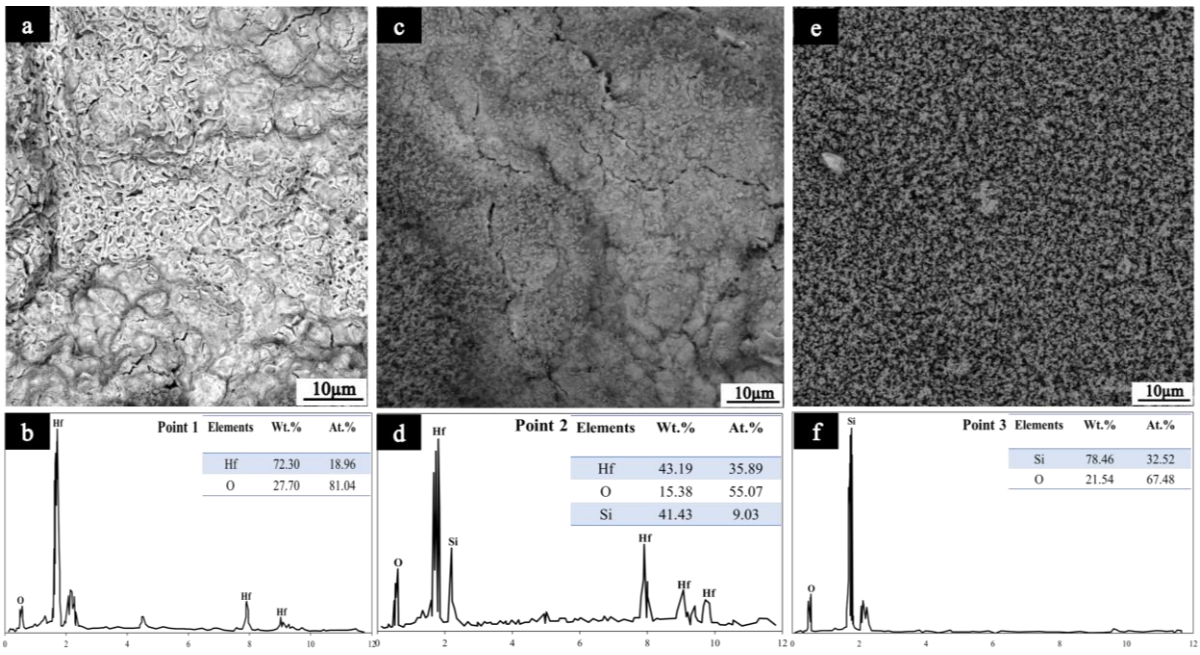

Fig. 9. SEM-BSE micrographs and EDS analysis of the ablated parts of C/C-SiC-HfC composite under the oxyacetylene flame: a) central region, b) transitional region, and c) side region

[Downloaded from cehsat.iust.ac.ir on 2026-09-10]

[DOI: 10.22068/ijmse.4552]

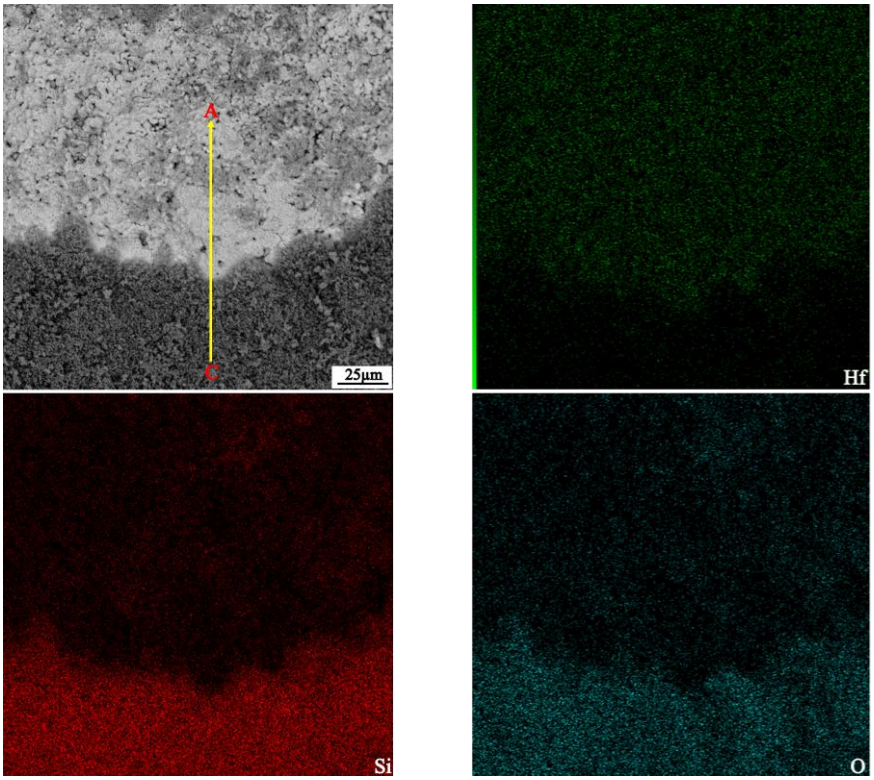

Fig. 10. SEM micrograph and the EDS maps of elements of the C/C-SiC-HfC composite

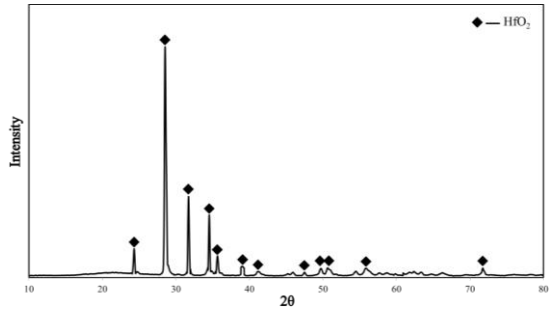

Fig. 11. XRD pattern of the central region of the C/C-SiC-HfC composite after the oxyacetylene test

The following reactions may occur during the ablation test under an oxyacetylene gas flame in region A:

$C\ (s) + O_2\ (g) \rightarrow CO_2\ (g)$ (1)

$2C\ (s) + O_2\ (g) \rightarrow CO\ (g)$ (2)

$CO\ (g) + O_2\ (g) \rightarrow CO_2\ (g)$ (3)

$SiC\ (s) + O_2\ (g) \rightarrow SiO_2\ (l) + CO\ (g)$ (4)

$SiC\ (s) + CO_2\ (g) \rightarrow SiO_2\ (l) + CO\ (g)$ (5)

$SiO_2\ (l) + CO\ (g) \rightarrow SiO\ (g) + CO_2\ (g)$ (6)

$SiO_2\ (l) + C\ (s) \rightarrow SiO\ (g) + CO\ (g)$ (7)

$SiO_2\ (l) \rightarrow SiO_2\ (g)$ (8)

$HfC\ (s) + O_2\ (g) \rightarrow HfO_2\ (s) + CO\ (g)$ (9)

$HfC\ (s) + CO_2\ (g) \rightarrow HfO_2\ (s) + CO\ (g)$ (10)

$HfO_2\ (s) \rightarrow HfO_2\ (l)$ (11)

By combining Fig. 9, Fig. 10, and Fig. 12, it can be found that the minor wear in region A is probably due to thermochemical corrosion and thermomechanical wear. Fig. 12 shows the ablation mechanism of the C/C-SiC-HfC composite. Region A experiences the highest pressure, velocity, and temperature of the oxyacetylene flame (2500°C) immediately, and the constituent phases of the composite, including HfC, SiC, carbon fibers, and matrix carbon (caused by the PIP and I-CVI processes), get in direct contact with oxide gases (Eqs. 1 to 11). In the early stages of the oxyacetylene flame test, carbon phases are rapidly oxidized and exit the composite surface (Eqs. 1 to 3). With an increase in both the test time and oxyacetylene flame temperature, HfC, and SiC carbide phases react with oxygen at 1100°C and 1600°C, respectively, and convert to HfO_2 and SiO_2 according to Eqs. 4, 5, 9, and 10. SiO_2 and HfO_2 act as barriers against the diffusion of oxygen to the inner layers of the preform. When the temperature is beyond 1415°C, the SiO_2 phase starts to melt and evaporate owing to the high pressure of combustion gases (Eqs. 6 and 7). At 1600°C, HfC particles convert to the HfO_2 continuous oxide layer. Because of its very high melting point (2785°C), HfO_2 covers the composite surface in the form of a monolithic viscous layer of HfO_2-SiO_2.

[Downloaded from cehsat.iust.ac.ir on 2026-09-10]

[DOI: 10.22068/ijmse.4552]

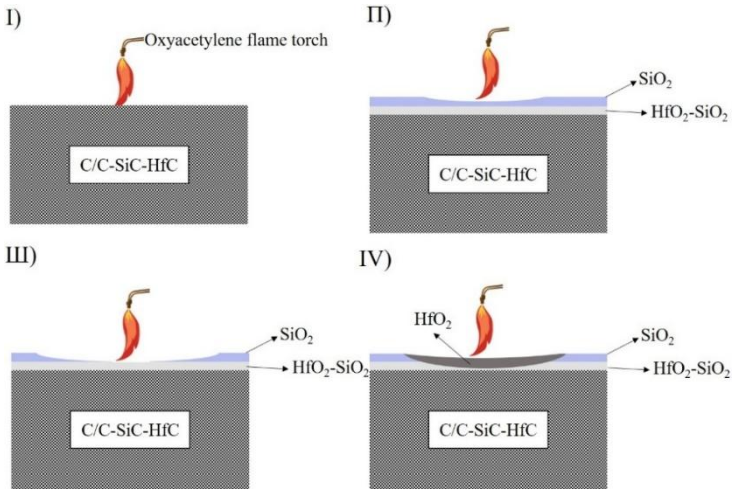

Fig. 12. Surface ablation mechanism of the C/C-SiC-HfC composite

Thus, the HfO_2 layer is a high-strength coating with high adhesion to the surface, acting as a barrier against the diffusion of oxygen to the bulk parts of the composite, which results in a decrease in the mass and linear ablation rates. The results obtained in this research are in agreement with this conclusion [32, 33]. The significant ablation behavior of the C/C-SiC-HfC composite, compared with that of similar studies, is because of a novel 3D orthogonal preform as well as a new combined fabrication method.

4. CONCLUSIONS

A novel 3D orthogonal C/C-SiC-HfC composite was fabricated through a new I-CVI, SI, and LSI combined method, including the penetration of carbon by I-CVI, the impregnation of phenolic resin and HfC particles by SI, and the infiltration of Si alloy at 1650°C by LSI. The oxyacetylene flame test calculated the mass and linear ablation rates of the composite. The as-fabricated C/C-SiC-HfC composite exhibited a much higher ablation resistance than C/C-SiC and C/C-SiC-HfC [13] composites. The mass and ablation rates of the C/C-SiC-HfC composite after the oxyacetylene flame test for 120 s were 1.6 mg/s and 0.98 μm/s, respectively. The residual Si and matrix SiC were rapidly oxidized, melted, and evaporated under the high pressure and temperature of the oxyacetylene flame, and exited the surface. HfC ultra-high temperature ceramic particles could significantly decrease the mass and linear ablation rates through the formation of a dense HfO_2 glass layer and covering the surface. The dense continuous HfO_2 layer, with a high melting point, could act as a strong barrier against the diffusion of oxygen to the bulk parts of the C/C-SiC-HfC composite, leading to a significant decrease in the ablation rate and oxidation of the composite.

ACKNOWLEDGMENT

The authors are deeply grateful to Professor Malek Naderi for his constructive suggestions and for providing the necessary resources and laboratory facilities that made this research possible. His profound expertise and encouragement have been instrumental in the completion of this study.

REFERENCES

[1] Squire, TH. and Marschall, J., “Material property requirements for analysis and design of UHTC components in hypersonic applications”. J. Journal of the European Ceramic Society. 2010, 30, 2239‑2251.

[2] Kyu-Seop, K., Sea-Hoon, L., Van Quyet, N., Yongtae, Y., and Sejin, K., “Ablation characteristics of rocket nozzle using HfC-SiC refractory ceramic composite”. J. Acta Astronautica. 2020, 31-44.

[3] Chenghai, X., Fajun, Y., Songhe, M., Yanyan, H., Xinxing, H., and Qiang, Y. “Compressive experimental method and properties of C/C composites under ultra-high temperature environment”. J. Journal of the European Ceramic Society. 2022, 4702-4711.

[4] Jacobson, N. S. and Curry, D. M., “Oxidation microstructure studies of reinforced carbon/carbon”. J. Carbon. 2006, 1142–1150.

[Downloaded from cehsat.iust.ac.ir on 2026-09-10]

[DOI: 10.22068/ijmse.4552]

[5] Bruneton, E., Narcy, B., and Oberlin, A., "Carbon-carbon composites prepared by a rapid densification process II: structural and textural characterizations". J. Carbon. 1997, 1599–1611.

[6] Yi-ang, Sh., Bai-lin, Z., Qing-dong, S., Jin-jin, W., and Si-ye, L., "Thermal performance and ablation characteristics of C/C-SiC for thermal protection of hypersonic vehicle". J. Journal of the European Ceramic Society. 2021, 5427-5436.

[7] Rubio, V., Ramanujam, P., and Cousinet, S., "Thermal properties and performance of carbon fiber-based ultra-high temperature ceramic matrix composites (Cf-UHTCMCs)". J. J Am Ceram Soc. 2020, 103: 3788–3796.

[8] Wu, H., Li, H. J., Fu, Q.G., and Yao, D.J., "Microstructure and ablation resistance of ZrC coating for SiC coated carbon/carbon composites prepared by supersonic plasma spraying". J. J Therm. Spray Technol. 2011, 1286-1291.

[9] Ma, Q. and Cai, LH., "Fabrication and oxidation resistance of mullite/yttrium silicate multilayer coatings on C/SiC composites". J. J Adv Ceram. 2017, 6: 360‑367.

[10] Xu, Y., Zhang, L.T., and Cheng, LF., "Microstructure and mechanical properties of three-dimensional carbon/silicon carbide composites fabricated by chemical vapor infiltration". J. Carbon. 1998, 36: 1051‑1056.

[11] Krenkel, W. and Berndt, F., "C/C‑SiC composites for space applications and advanced friction systems". J. Mat Sci Eng. 2005, 412: 177‑181.

[12] Wang, Y.J., Li, H.J., Fu, Q.G., Wu, H., and Yao, D.J., "Ablative property of HfC-based multilayer coating for C/C composites under oxyacetylene torch". J. Appl Surf Sci. 2011, 4760-4763.

[13] Zhiqiang, L., Yujun, J., Shubo, Zh., Jian, Zh., Jingtong, L., Luncheng, T., Jiaping, Zh. and Qiangang, Fu., "Ablation resistance and mechanical properties of C/C-HfC-SiC composites with a bulletproof-like layer". J. Ceramics International. 2024, 49480-49489.

[14] Liuyang, D., Xing, Zh., and Yiguang, W., "Comparative ablation behaviors of C/SiC-HfC composites prepared by reactive melt infiltration and precursor infiltration and pyrolysis routes". J. Ceramics International. 2017, 16114-16120.

[15] Zhigang, Zh., Kezhi, L., Wei, L., and Leilei, Zh., "Cyclic ablation behavior of C/C-ZrC-SiC-ZrB_2 composites under oxy-acetylene torch with two heat fluxes at the temperatures above 2000°C". J. Corrosion Science. 2021, 109202.

[16] Zhenxiao, T., Maozhong, Y., Huan, Y., Yuhui, D., Huang, W., and Peng, K., "Ablation behavior of a C/C-ZrC-SiC composite based on high-solid-loading slurry impregnation under oxyacetylene torch". J. Journal of the European Ceramic Society. 2022, 4748-4758.

[17] Li, B., Li, H.J, Yao, X.Y., Tian, X.F., Jia, Y.J. and Feng, G.H., "Ablation behavior of $(ZrC/SiC)_3$ alternate coating prepared on sharp leading-edge C/C composites by CVD". J. Journal of Materials Science & Technology. 2022, 129-139.

[18] Ping, T., Liyong, T., Steven, G.P., and Takashi, I., "Behavior of 3D orthogonal woven CFRP composites". Experimental investigation, Composites: Part A. 2000, 259–271.

[19] Xu, H., Zhang, L., and Cheng, L., "The effect of Z-yarn density on the in-plane shear property of three-dimensional stitched carbon fiber reinforced silicon carbide composites". J. Comp Sci Technol. 2015, 106:120–126.

[20] Mei, H., Liang, C., Zhang, D., Chen, C., and Cheng, L., "Controlled deposition of density defects for understanding mechanical reduction on 2D C/SiC composites". J. Comp Part B. 2019, 161:241–251.

[21] Niranjan, P., Nasrin, A. N., Daniel, D., and Jayaseelanb, W., "Thermal properties of Cf/HfC and Cf/HfC-SiC composites prepared by precursor infiltration and pyrolysis". J. Journal of the European Ceramic Society. 2018, 2297-2303.

[22] Qinchuan, H., Hejun, L., Qing, T., Jinhua, L., and Xuemin, Y., "Effects of ZrC particle size on ablation behavior of C/C-SiC-ZrC composites prepared by chemical liquid vapor deposition". J. Corrosion Science. 2022, 110469.

[23] Liuyang, D., Lei, L., Liping, L., and Yiguang, W., "Ablation of C/SiC–HfC composite prepared by precursor infiltration and pyrolysis in plasma wind tunnel". J. Journal of Advanced Ceramics. 2020, 9(3): 0‑0.

[Downloaded from cehsat.iust.ac.ir on 2026-09-10]

[DOI: 10.22068/ijmse.4552]

[24] Yiguang, W., Xiaojuan, Z., Litong, Z., and Laifei, Ch., "C/C–SiC–ZrC composites fabricated by reactive melt infiltration with $Si_{0.87}Zr_{0.13}$ alloy". J. Ceramics International. 2012, 4337–4343.
[25] Huilong, P., Shangwu, F., and Yiguang, W., "C/SiC–ZrB_2–ZrC composites fabricated by reactive melt infiltration with $ZrSi_2$ alloy". J. Ceramics International. 2012, 6541 6548.
[26] Seyoung, K., In Sub, H., Young-Hoon, S., and Kyung, K., "Mechanical properties of C–SiC composite materials fabricated by the Si–Cr alloy melt-infiltration method". J. Journal of Composite Materials. 2015, 3057–3066.
[27] Xiaoyang, J., Qing, T., Qinchuan, H., Mingcong, Q., Yiqun, W., and Xuemin, Y., "Cyclic ablation behavior of mullite-modified C/C-HfC-SiC composites under an oxyacetylene flame at about 2400°C". J. Journal of the European Ceramic Society. 2023. 4309-4321.
[28] Zhiqiang, L., Yujun, J., Jiaqi, H., Ruoxi, Z., Shubo, Zh., Jiaping, Zh., and Qiangang, Fu., "C/C-HfC-SiC composites with simultaneous resistance to ultra-high temperature airflow erosion and high temperature oxidation". J. Journal of Materiomics. 2025, 100846.
[29] Tulbez, S., Esen, Z., and Dericioglu, AF., "Effect of CNT impregnation on the mechanical and thermal properties of C/C-SiC composites". J. Adv Comp Hybrid Mater. 2020, 3(2):177–186.
[30] Mei, H. and Cheng, L., "Comparison of the mechanical hysteresis of carbon/ceramic-matrix composites with different fiber preforms". J. Carbon. 2009, 47(4):1034–1042.
[31] Du, X., Li, D., Wei, QH., and Jiang, L., "High temperature bending properties and failure mechanism of 3D needled C/SiC composites up to 2000°C". J. J Eur Ceram Soc. 2022, 42(6):3036–3043.
[32] Ke-Zhi, L., Tao, D., Jia-Ping, Zh., Ning-Kun, L., and Mao-Yan, Zh., "Ablation Mechanism of Carbon/Carbon Composites Modified by HfC–SiC in Two Conditions under Oxyacetylene Torch". J. Journal of Materials Science & Technology. 2017, 71-78.
[33] Xiaoyang, J., Qinchuan, H., Qing, T., and Xuemin, Y., "Ablation behavior of mullite modified C/C-SiC-HfC composites under oxyacetylene torch for single and cyclic ablations with two heat fluxes". J. Journal of the European Ceramic Society. 2023, 5851-5862.

[Downloaded from cehsat.iust.ac.ir on 2026-09-10]

[DOI: 10.22068/ijmse.4552]